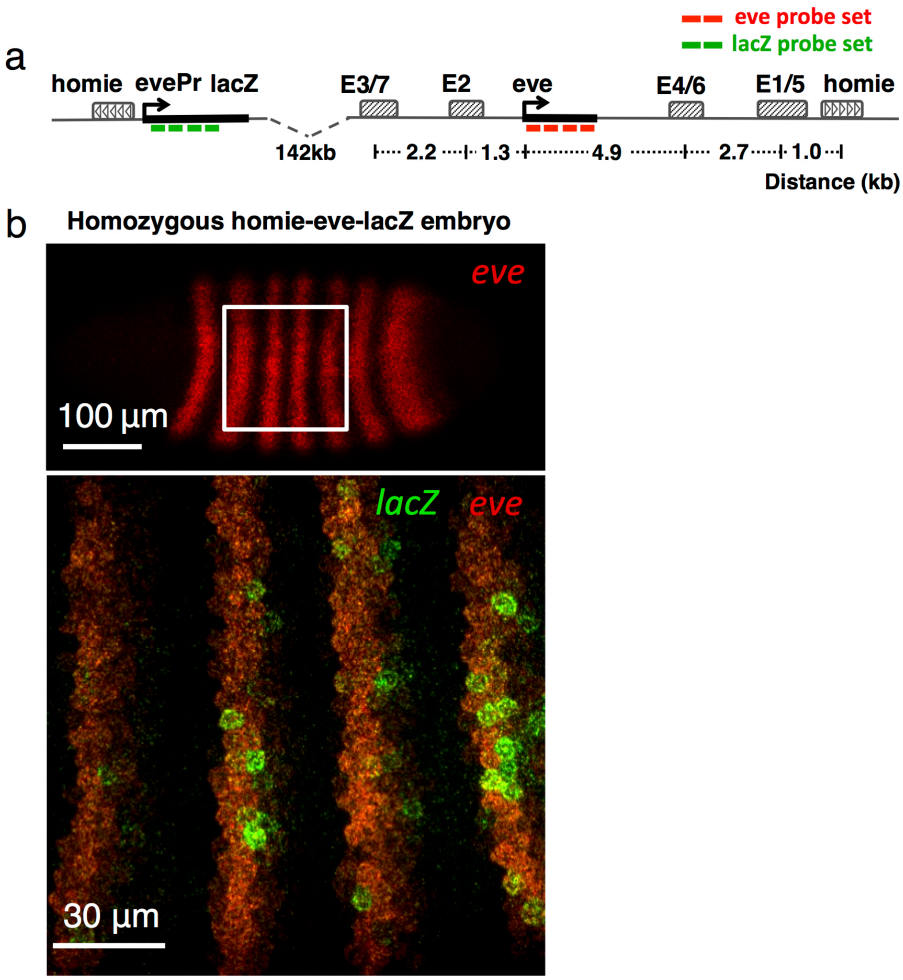

Supplementary Figure 1

Fluorescent in-situ hybridization (FISH) reveals *eve* enhancer-dependent expression of a reporter gene located 142kb upstream of the endogenous eve locus.

a, Genomic design of a synthetic long-range enhancer-promoter interaction. Ectopic *homie* insulator sequence with an *eve* promoter driving *lacZ* is integrated at ~142kb upstream of the *eve* locus. Embryos homozygous for this construct are hybridized with single molecule FISH probes to label endogenous *eve* (red) and *lacZ* (green) mRNA. **b,** Upper panel: surface view of a 2.5 h old Drosophila embryo hybridized with *eve*-atto633 probes. Anterior to the left. Lower panel: z-stack projection of the marked region in the upper panel. *LacZ* activity (labeled with *lacZ*-atto565 probes) only occurs sporadically within the limits of the *eve* pattern (red). This *lacZ* pattern appears in all 13 embryos imaged (2-3 h old) and a representative sample is shown here.

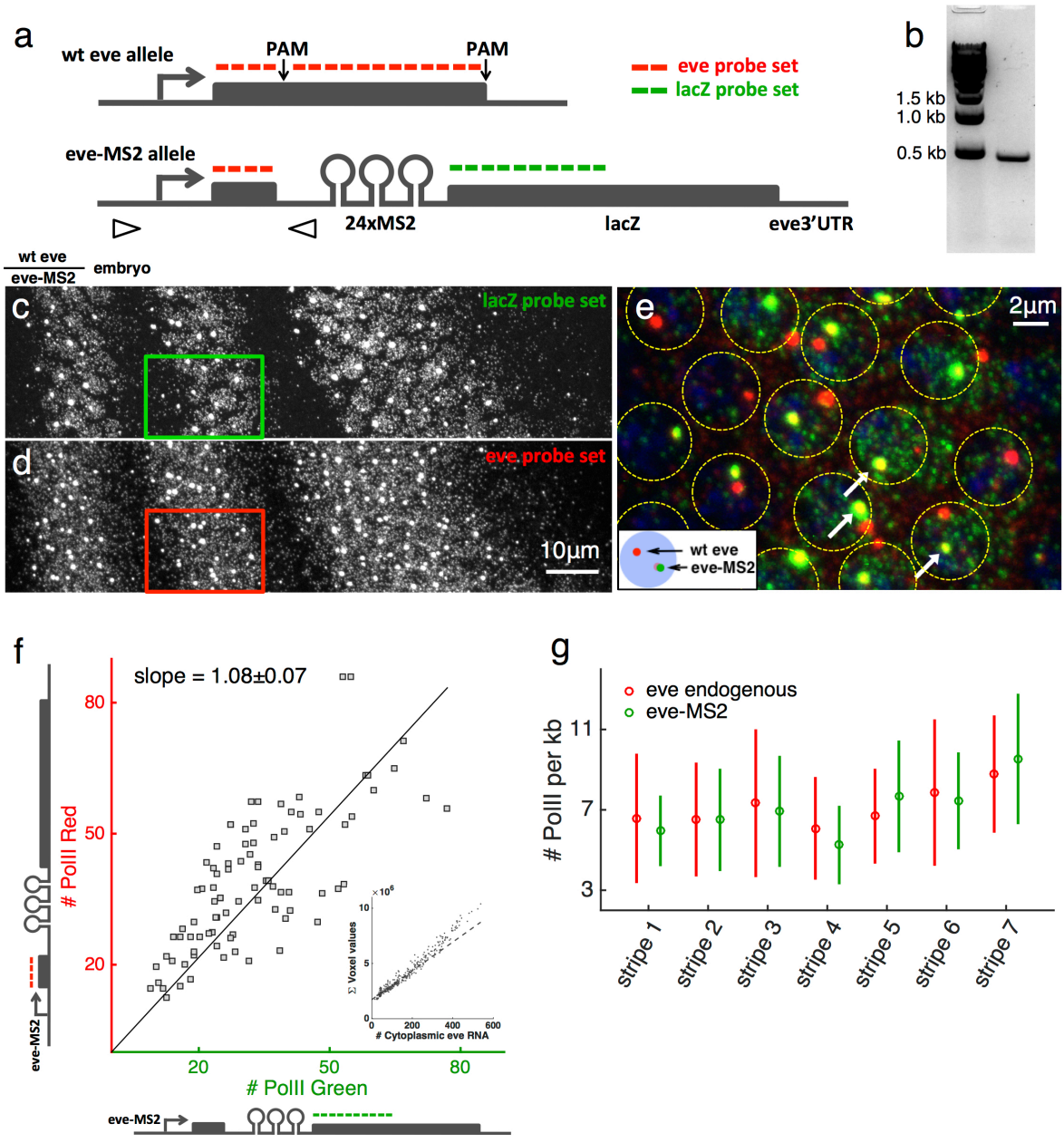

Supplementary Figure 2

The *eve*-MS2 allele recapitulates the expression pattern and transcriptional activity of the endogenous *eve* gene.

a, Editing the endogenous *eve* locus (upper) to obtain the *eve*-MS2 allele (bottom). Arrowheads indicate primers for PCR genotyping. Green and red lines mark sequences targeted by smFISH probes (*lacZ*-atto565 and *eve*-atto633, respectively). Loci not drawn in scale. **b,** Genotyping the *eve*-MS2 allele. PCR result from a single fly carrying the *eve*-MS2 allele is shown with the DNA ladder. The 466 base pair band is verified by sequencing. Primers are shown in **a**. **c-g,** smFISH quantification of the transcriptional activity of the *eve*-MS2 allele from a representative embryo at ~45 min into nc14. Maximum Z-projections are shown for *lacZ*-atto565 channel **(c)** and *eve*-atto633 channel **(d)** of an *eve*-MS2/*eve*$^{+}$ embryo. *eve* stripes 5 to 7 (from left to right) are shown. **e,** Magnified view of square in **c** and **d**. Nuclear regions are marked with yellow dashed lines. Arrows indicate examples of *eve*-MS2 transcription loci that are labeled by both probes. **f,** Cytoplasmic spots and active transcription spots are identified by image analysis routines (see Methods). A cytoplasmic unit (CU) that corresponds to fluorescent intensity of a single cytoplasmic mRNA is extracted. Panel shows number of RNA polymerase II (PolII) on the *eve*-MS2 loci from 93 nuclei in which a transcription spot in the *eve*-atto633 channel is observed at the *eve*-MS2 locus.

The PolII numbers are inferred from either the CU derived from *lacZ*-atto565 (x-axis) or from eve-atto633 (y-axis) measurements. Inset shows calculation of cytoplasmic unit for *eve*. Specifically, a sliding window of 220x220x23 pixel (16.5x16.5x7.4 μm^3) is applied to the raw image stack (**c** and **d**) and the total pixel values in the window are plotted against the number of cytoplasmic spots found in the window. A linear fit in the range of 0-100 cytoplasmic spots is applied to extract CU for each probe set. **g,** Comparison of the PolII number on the *eve*-MS2 locus and on the endogenous *eve* locus (Mean±STD). Note that the numbers reported in **f** and **g** are for two sister chromatids. Number of nuclei analyzed for stripes 1 to 7 is 25, 28, 24, 23, 25, 27 and 54, respectively. Analysis performed on other embryos (n=3) imaged at different stages in nc14 also shows no significant difference of PolII numbers on the *eve*-MS2 locus and on the endogenous *eve* locus.

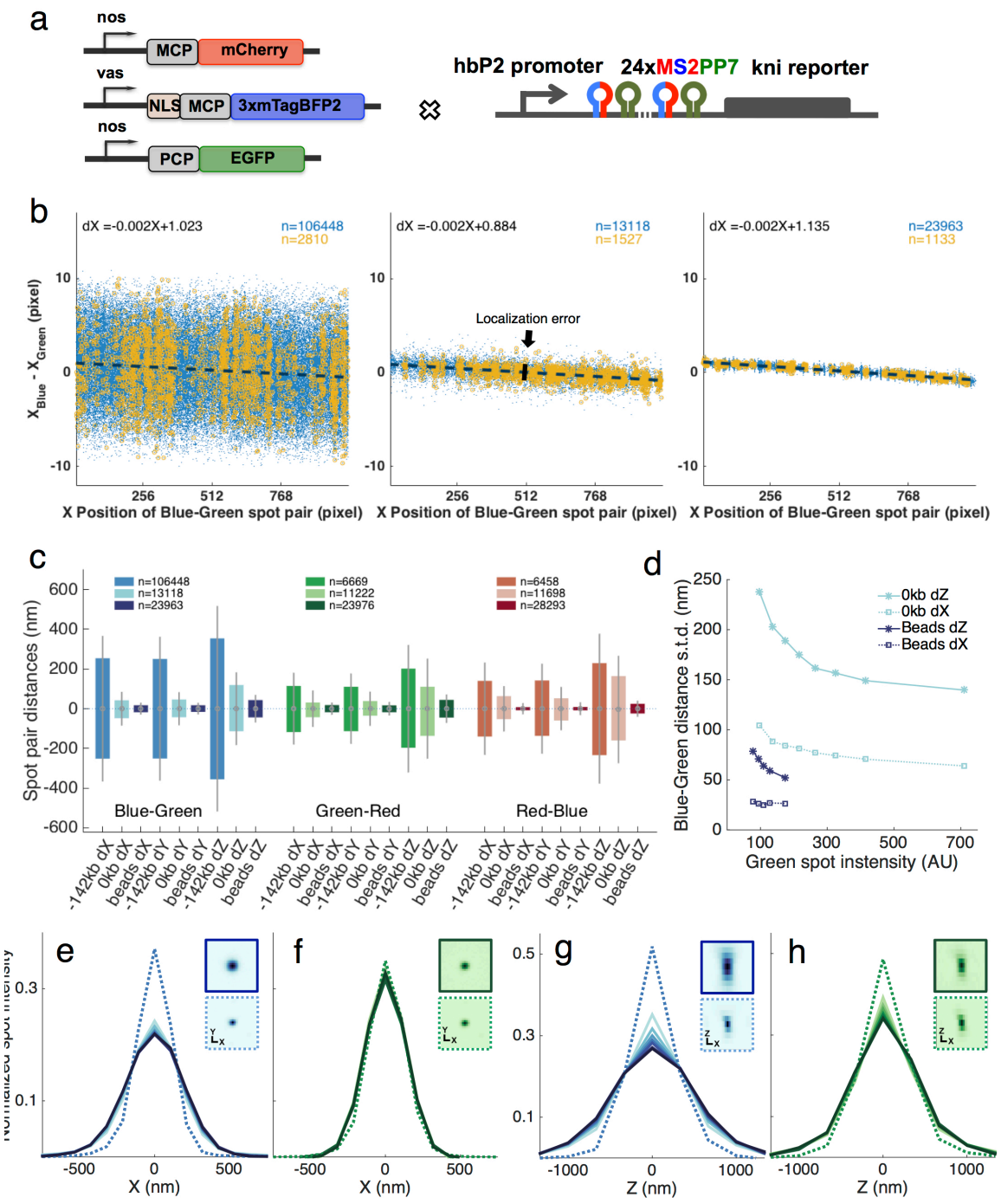

Supplementary Figure 3

Spot localization precision and measurement error.

a, Genetic design of a transgene that co-localizes all three reporter systems. MS2 and PP7 stem loops are alternated and repeated 24 times. A *knirps* (*kni)* reporter gene, which includes *kni* CDS (with the start codon removed) and 3'UTR, is driven by a hunchback P2 (hbP2) promoter, resulting in expression in all nuclei located in the anterior 10–45% of the embryo. **b,** Analysis of chromatic aberration and localization error (see Methods for details). Panels show the linear distance (along x-coordinate only) for each blue-green spot pair as a function of the pair's x-position for *eve-MS2* embryos carrying the *parS-homie-eve-PP7* transgene (left, n=34 embryos), embryos

carrying the three-color co-localization transgene from **a** (middle, n=9 embryos), and TetraSpec beads (right, n=5 independent data sets), respectively. Blue data points are for all spot pairs at all time frames for all embryos analyzed. Yellow data points are from one of the embryos (or one set of experiment for the beads). Linear fits in each panel report on the chromatic aberrations between blue and green spots in the x-direction. As slopes and intercepts for the different samples show no significant differences, chromatic aberrations can be corrected for each individual embryo data set internally. **c,** Summary of the distributions of spot pair distances (after chromatic aberration correction) for the three configurations in **b**. Each direction (x, y, and z) is shown for each color combination. For example, for the blue-green (MS2-parS) distances in the x-direction the STD of the *parS-homie-eve-PP7* transgene (labeled -142kb) corresponds to the solid black bar shown in the left panel of **b**. Spot localization errors are estimated from the STDs measured with the three-color co-localization control embryos (labeled 0kb). Center values: means; Solid lines: STDs; bars: 25%-75% quantiles. **d,** Dependence of localization precision on signal intensities. Since localization precision scales directly with the square root of the number of photons, we can assess localization error of the three-color co-localization control embryos from the localization error measured with immobilized beads of the similar fluorescent intensity values (photon counts). Thus the differences in y-axis offset are not due to differences in photon counts, but due to *motion blurring* of the moving spot during acquisition, which amounts to about 2/3 of the total localization. The remaining 1/3 (corresponding to the error obtained from immobile beads) stems from optical measurement noise and our analysis pipeline. **e-h,** Optical characterization of nascent transcription sites and parS foci. For each fluorescent channel, all identified fluorescent spots are classified into eight groups according to their raw intensities. A *super-spot* for each group is obtained by aligning all spots of a group with the brightest pixel at the center of a 25x25x13 voxel region-of-interest and by taking the average intensity per voxel in that region over all spots. The intensity profiles along the X- (**e**, **f**) and Z-cross-sections (**g**, **h**) for the blue MS2 *super-spot* (**e**, **g**) and green parS *super-spot* (**f**, **h**) are plotted (darker curves represent brighter spots). Dashed lines are from equivalent measurements of TetraSpec beads. Images of the *super-spots* for the brightest blue (MS2, **e** and **g**) or green (parS, **f** and **h**) spots (upper) and for the beads (lower) are shown as panel insets.

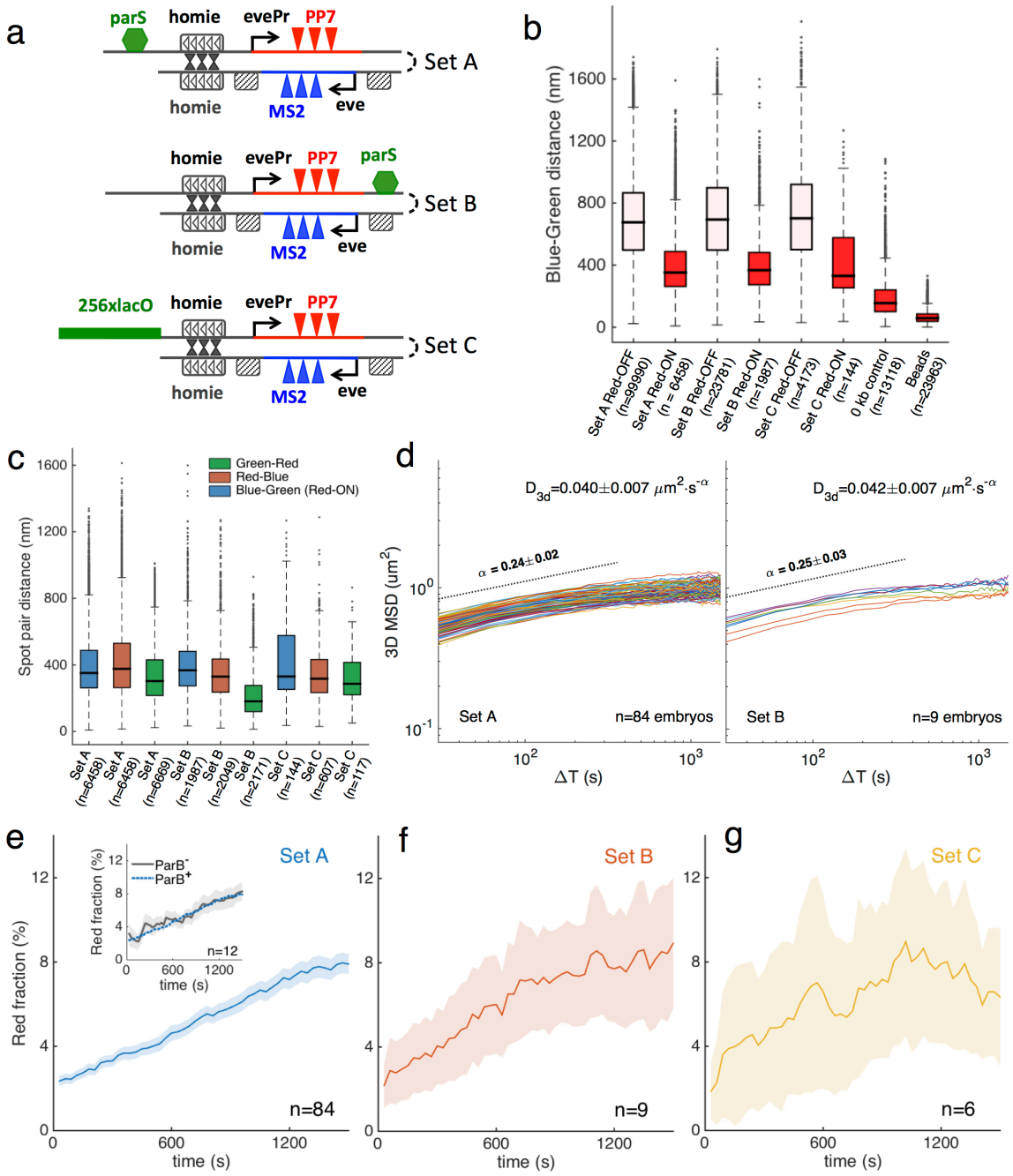

Supplementary Figure 4

Different genomic labeling approaches report on similar chromatin dynamics and transcription kinetics.

a, Three methods of labeling genomic loci. **b,** The measured Blue-Green (MS2-parS) distances are not sensitive to labeling approaches. Boxplot showing distributions of the instantaneous distance between spot pairs in the same nuclei. Distances shown are after chromatic aberration corrections. For all three genomic settings, the MS2-parS (blue-green) distances show no significant differences (one-way Kruskal–Wallis test on individual embryo mean distances, n=34, 9 and 6 embryos for Set A, B and C, respectively). This is observed regardless the absence (Red-OFF, p=0.17, chi^2=4.3, df=50) or presence (Red-ON, p=0.60, chi^2=1.04, df=49) of *PP7* activity. Center values: medians; Boxes: inter quantile ranges (25%-75% quantiles); Whiskers: 1.5 times the inter quantile range. 0-kb control is the *hbP2-MS2PP7-kni* embryo described in Supplementary Fig. 3. **c,** The distances between spot pairs

reflect their genomic arrangement. Distributions of the instantaneous distance between spot pairs are plotted. Box and whiskers as in **b**. Distances shown are after chromatic aberration corrections. Notice that the parS-PP7 (green-red) distance is significantly shorter when the parS tag is located at the 3' side of the *PP7* reporter (p=4.5×10^{-6}, two-tailed Wilcoxon rank sum test). **d,** Mean square displacement (MSD) plots for Set A and Set B. Each MSD trace is a result of the population ensemble of all nuclei in a single embryo (embryo-averaged MSD, see Methods). Results from the two genomic settings display sub-diffusive characteristics with a scaling power of ~0.24, and their anomalous diffusion coefficients show no significant difference (two-tailed Student's t-test, p=0.87, t=-0.1534, df=90; linear fits with mean±STD across embryos). **e-g,** Transcriptional activation of *eve-PP7* is not affected by labeling approaches. The fraction of *eve*-MS2 expressing nuclei that also contain active PP7 (mean±SE) is plotted as a function of time for three genomic settings. It seems that neither the presence nor location of the parS tag interferes with either enhancer action or transcriptional activation. This is consistent with the hypothesis that the ParB-DNA complex is formed from specific ParB-parS nucleation sites followed by stochastic binding and trapping.

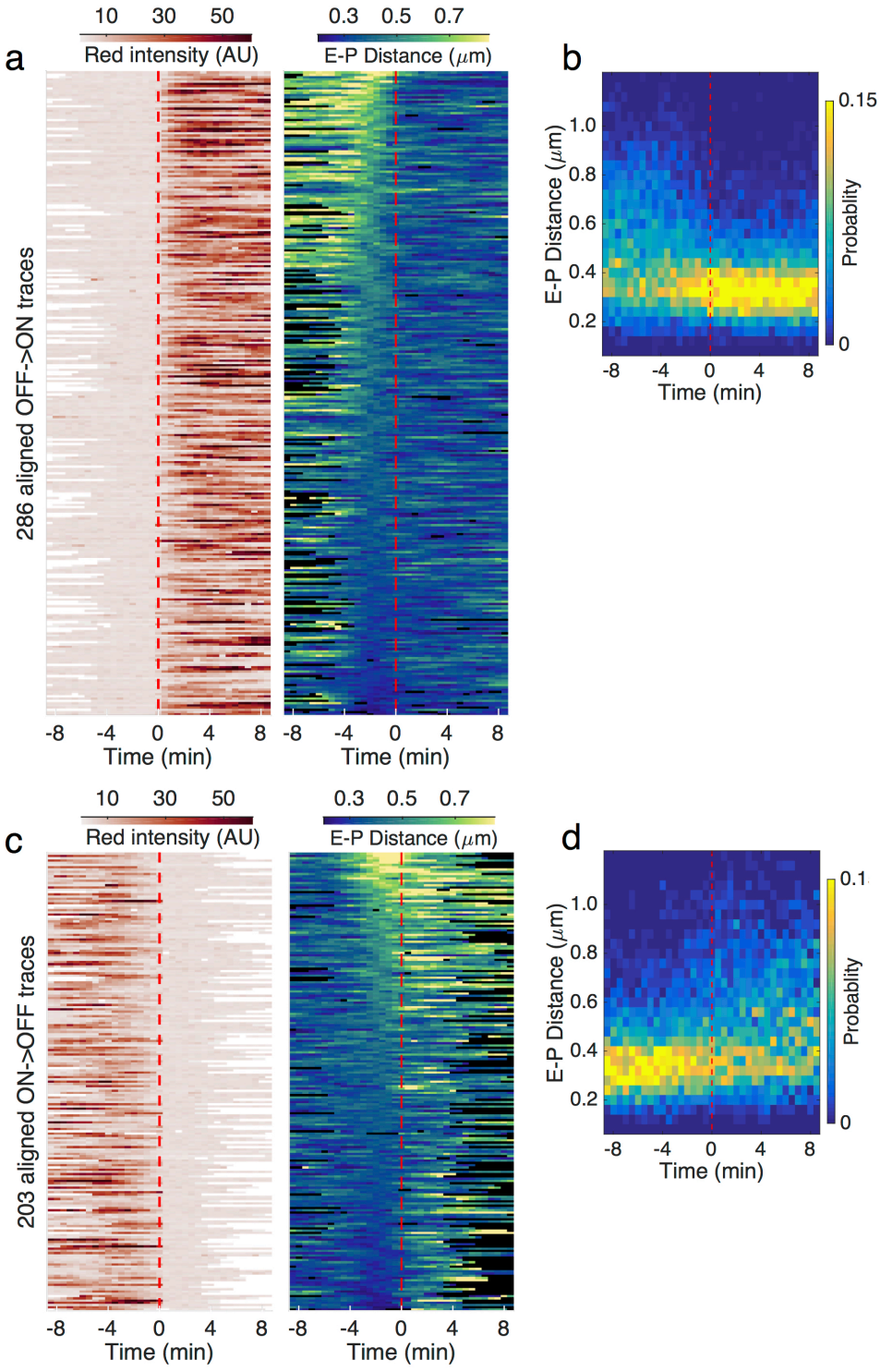

Supplementary Figure 5

Sustained physical proximity is required for transcription initiation and maintenance: individual traces.

a, Transcriptional activity (red spot (PP7) intensity) and instantaneous E-P distance (blue-green distance) as a function of time for 286 nuclei transitioning from Red-OFF to Red-ON state. Time series for individual nuclei are aligned such that PP7 activity starts at 0 min

(red dashed lines). Individual traces are sorted according to the mean E-P distance within the 5 min before PP7 activity is observed. **b,** Distribution of the instantaneous E-P distance as a function of time for the Red-OFF to Red-ON transition. Calculated from **a**. **c,** Transcription and instantaneous E-P distance as a function of time for 203 nuclei transitioning from Red-ON to Red-OFF state. Time series for individual nuclei are aligned such that PP7 activity ends at 0 min (red dashed lines). Individual traces are sorted according to the mean E-P distance within the 5 min before PP7 activity disappears. **d,** Distribution of the instantaneous E-P distance as a function of time for the Red-ON to Red-OFF transition. Calculated from **c**.

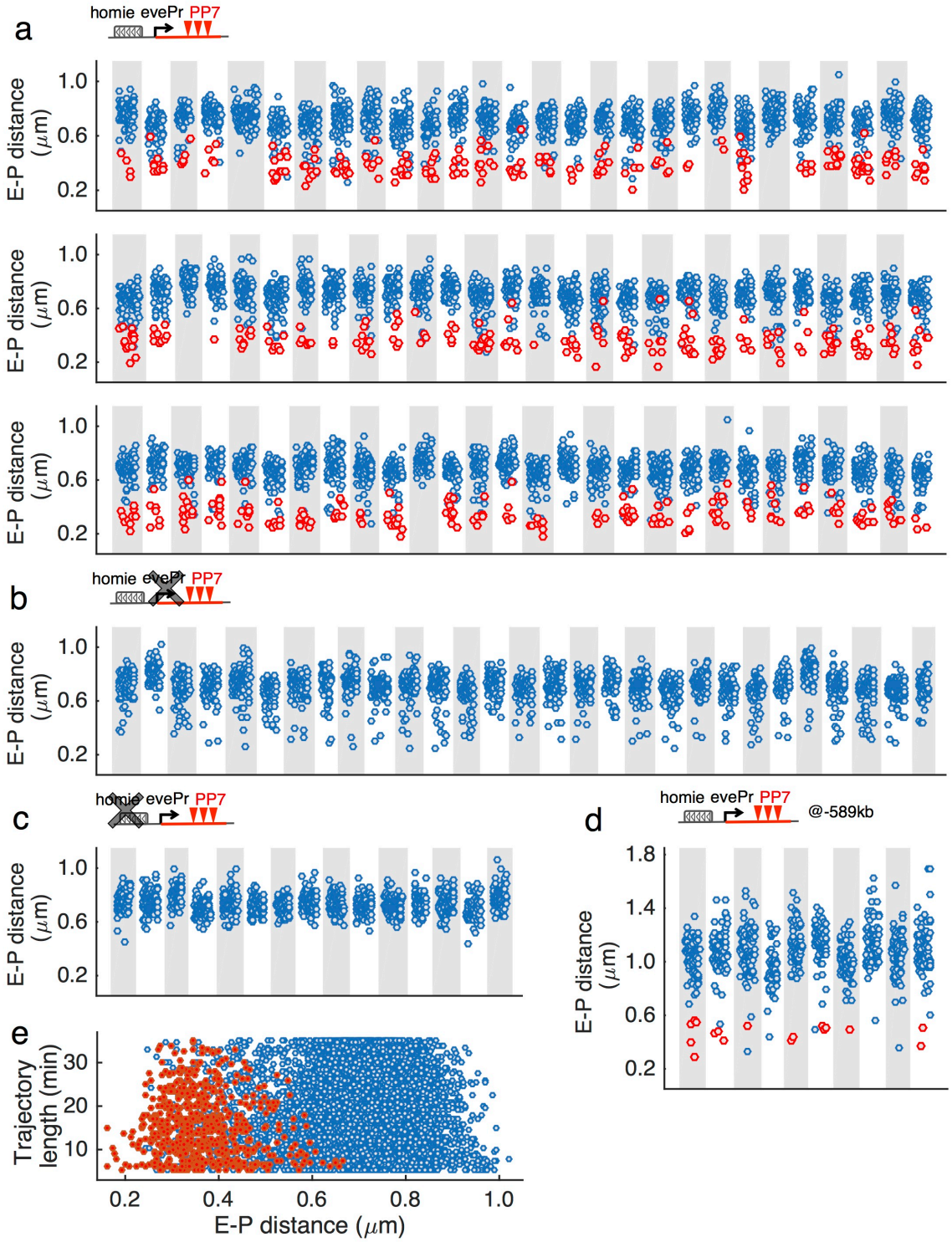

Supplementary Figure 6

Analysis of E-P distance for individual embryos and individual nuclei.

a-c, Time-averaged RMS distance between MS2 (blue) and parS (green) spots (E-P distance) is depicted as a scatter plot for each

nucleus from 84 embryos carrying the *parS-homie-evePr-PP7* construct (**a**), 29 embryos carrying the *parS-homie-noPr-PP7* construct (**b**), and 15 embryos carrying the *parS-lambda-evePr-PP7* construct (**c**) located at -142kb from the *eve-MS2* locus. **d,** Time-averaged RMS E-P distance for 10 embryos carrying the *parS-homie-evePr-PP7* construct at -589kb from the *eve-MS2* locus. Data points marked in red are calculated from the Red-ON part of E-P trajectories in nuclei displaying PP7 activity. Data points marked with blue are calculated from full E-P trajectories in nuclei that never show PP7 during the imaging time window (25–55 min in nc14). Notice that the number of time points (e.g. length of E-P trajectories) used for calculating RMS distance varies among nuclei depending on the nuclear A-P position and the view of image. **e,** RMS E-P distance as a function of the length of trajectories used for RMS distance calculation. All RMS E-P distance samples from the 84 embryos carrying the *parS-homie-evePr-PP7* construct at -142kb are shown.

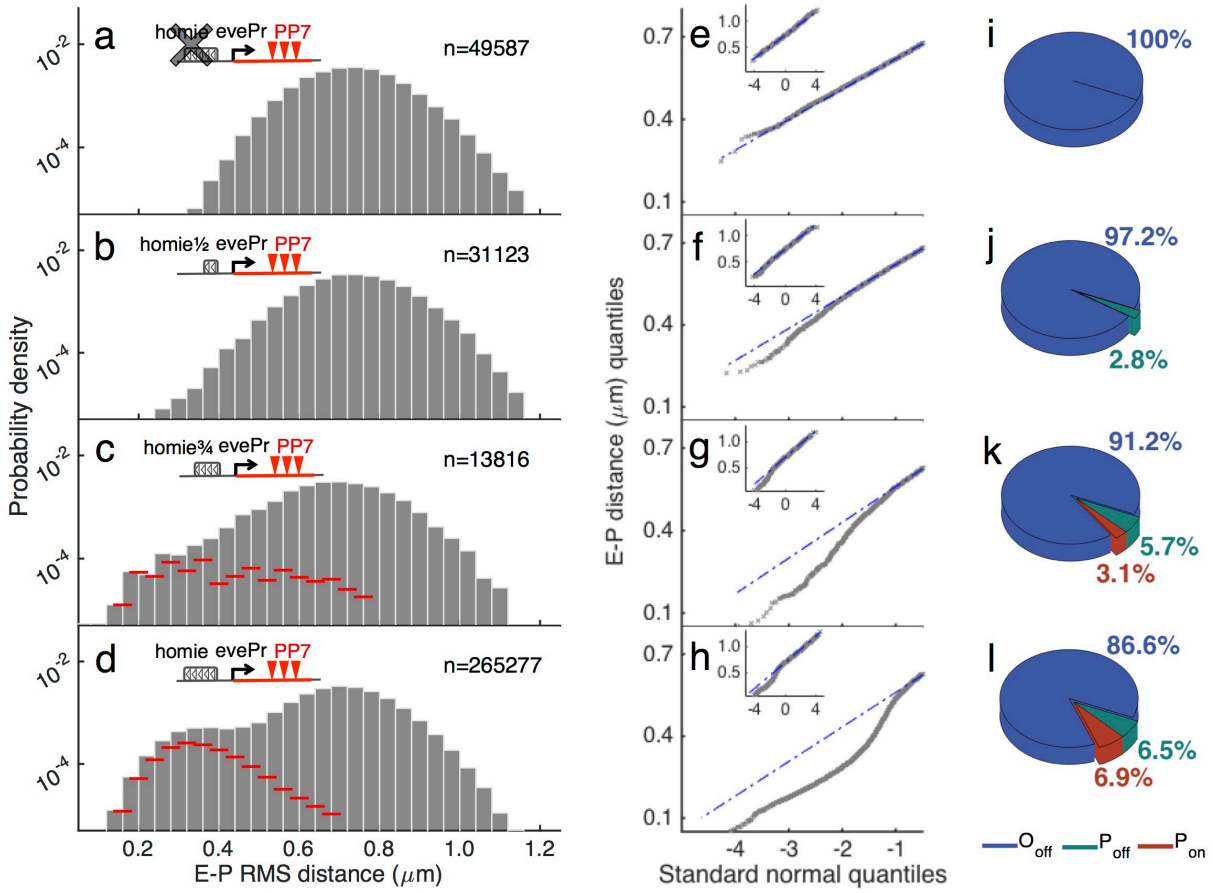

Supplementary Figure 7

Tuning stability of the *homie* element.

a-d, E-P distance (RMS distance) distribution for four experimental constructs: *parS-lambda-evePr-PP7, parS-homie½-evePr-PP7, parS- homie¾-evePr-PP7 and parS-homie-evePr-PP7*, respectively. A 5-min-sliding window along each time trace is used to calculate RMS E-P distances. *homie½* (chr2R:9,988,934..9,988,750, dm6) and *homie¾* (chr2R:9,989,025..9,988,750, dm6) are two truncated *homie* element. Red bars in (**c**) and (**d**) show the probability density of RMS distance samples accompanied by continuous PP7 transcription. **e-h,** Quantile-quantile (Q-Q) plots against standard normal distribution for the RMS E-P distance shown in (**a-d**), respectively. Short E-P distances resulting from the paired (P_{off} and P_{on}) states are progressively enriched as the stability of the *homie* element increases. Insets show the complete Q-Q plots. **i-l,** Fraction of each topological state for constructs shown in (**a-d**), respectively. See Supplementary Fig. 8 and Methods for details about topological state classification.

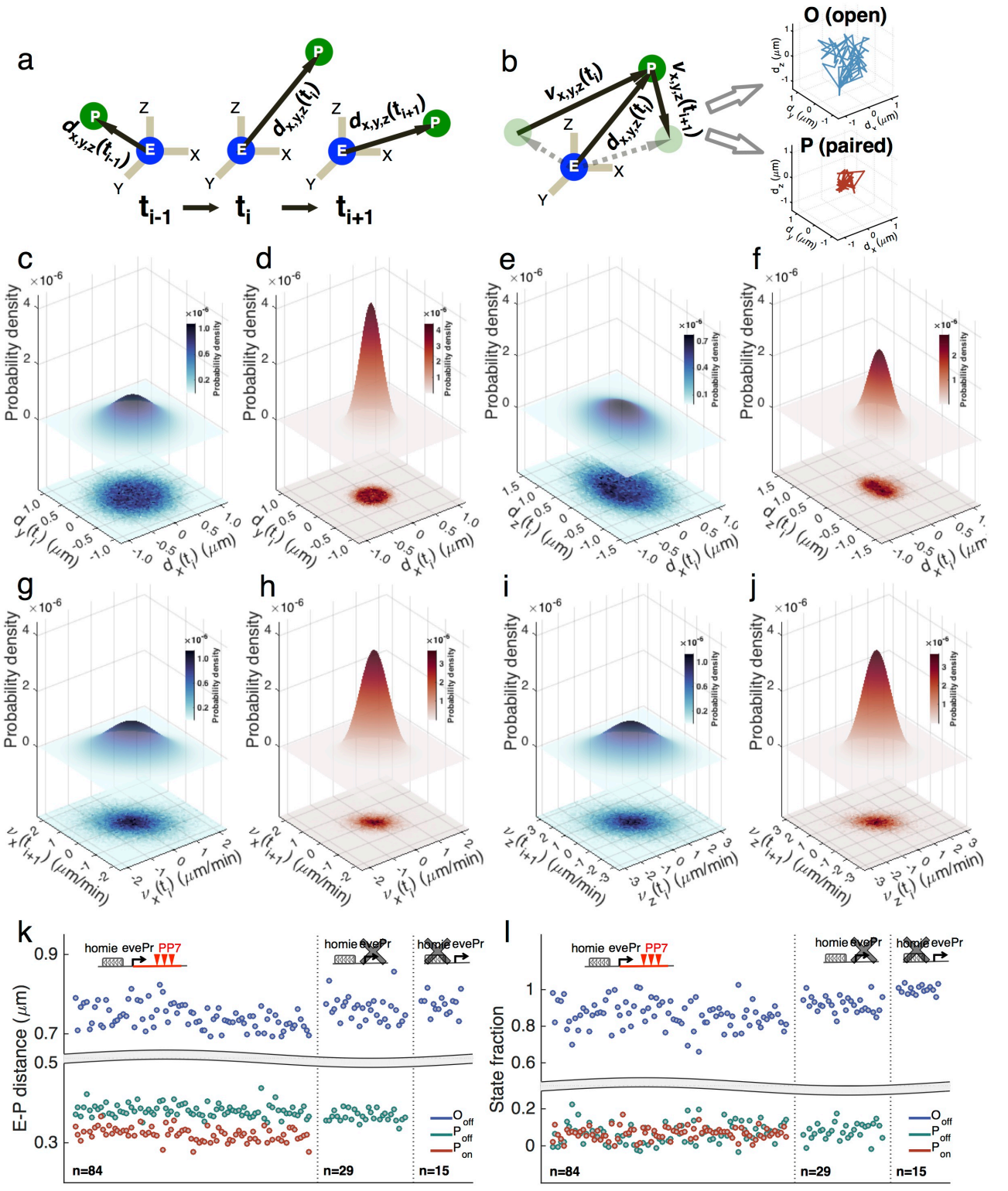

Supplementary Figure 8

Training of a Bayesian classifier and characterization of the three topological states.

a, E-P distance vector ($\boldsymbol{d}_{x,y,z}$) at each time point is calculated, corrected for chromatic aberration. **b,** The relative velocity ($\boldsymbol{v}_{x,y,z}$) between the enhancer (blue MS2 spot) and the promoter (green parS spot) is calculated from the two consecutive distance vectors. The instantaneous distance vector and the two velocity vectors that connect the two adjacent time points are used for training a binary classifier using a naïve Bayes method (see Methods). Two training samples are used. For the open state (O state), E-P trajectories from the *parS-lambda-evePr-PP7* control are used. For the paired state (P state), E-P trajectories from the Red-ON part of nuclei displaying PP7 activity are used. The last 4 min of these Red-ON trajectories are removed from the training sample due to PolII elongation. **c-f,** Joint distribution of the selected dimensions of the distance vectors for the O state (**c**, **e**) and P state training samples (**d**, **f**). **g-j,** Joint distribution of the selected dimensions of the velocity vectors for the O state (**g**, **i**) and P state training samples (**h**, **j**). From **c** to **j**, z-projections are raw data, and the probability density functions of two-dimensional Gaussian fits are shown. **k-l,** RMS distance (**k**) and fraction (**l**) of each topological state calculated for individual embryos (n=number of embryos).

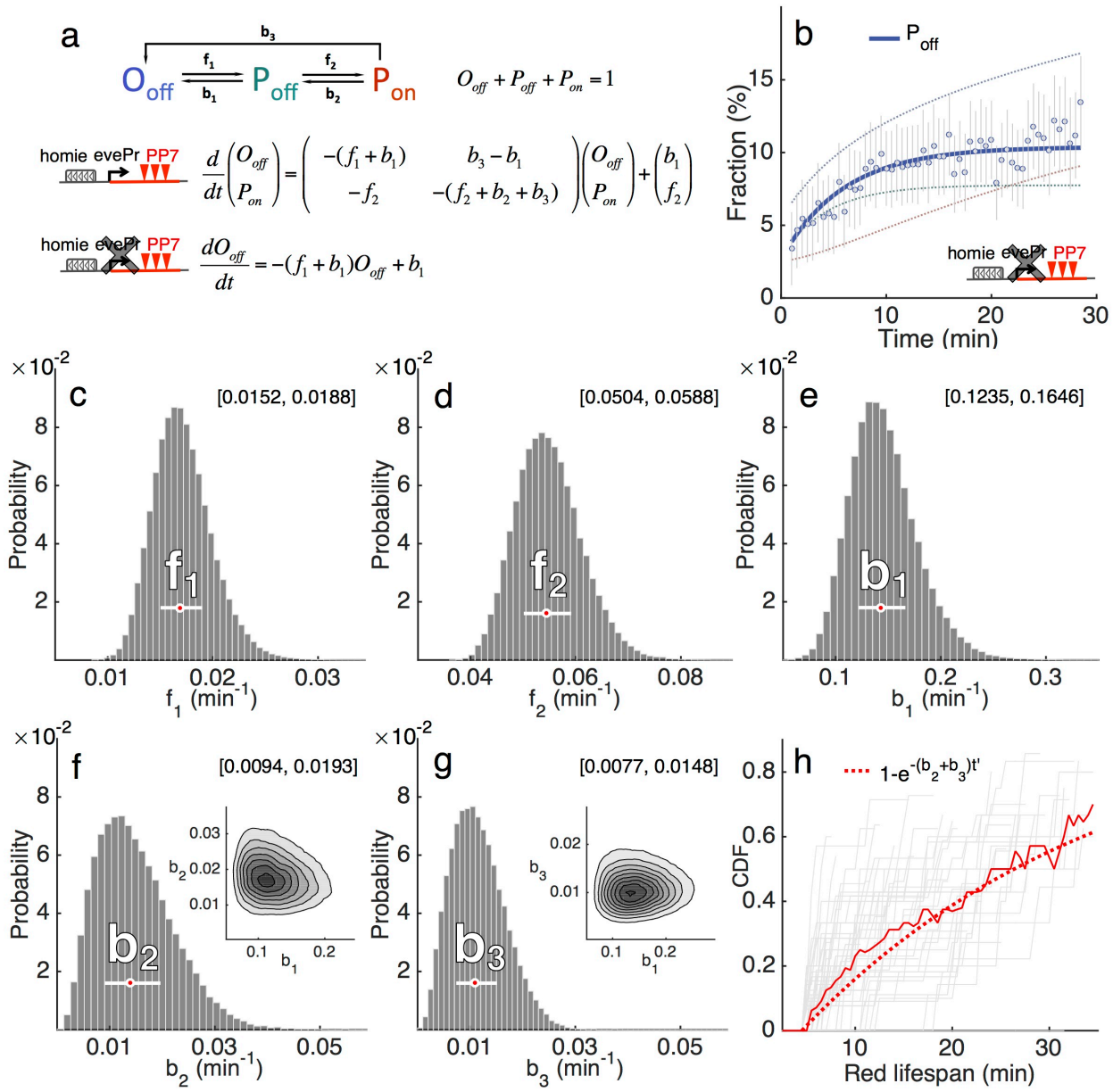

Supplementary Figure 9

Kinetic model captures transition rates among the three topological states.

a, A series of first order reactions are used to model the transition kinetics between the O_{off}, P_{off} and P_{on} states. Based on the finding that physical proximity is required for transcriptional activation, we assume in this model that P_{on} occurs only after P_{off} is established. The coupled ODEs describe evolution of the system given the initial conditions. For *parS-homie-noPr-PP7*, only O_{off} and P_{off} states are present, and we assume the same f_1 and b_1 as for *parS-homie-evePr-PP7*. **b,** Fraction of the P_{off} state for *homie-noPromoter-PP7* as a function of developmental time. 0 on the x-axis corresponds to 25 min in nc14. Mean±SE (n=29 embryos). This curve, together with time series curves obtained from the *parS-homie-evePr-PP7* construct (dashed lines, same as in Fig. 3e), is used to infer the kinetic parameters with Markov chain Monte Carlo (MCMC) simulations (see Methods). **c-g,** Marginal posterior distributions of the five kinetic parameters in **a** constructed from 90,000 stationary MCMC samples. Medians are labeled. Error bars span from the 25% to the 75% quantiles (also shown in square brackets). Insets in **f** and **g** show the joint distribution of (b_1, b_2) and (b_1, b_3), respectively. Darker color represents higher density. **h,** The inferred parameters for the disappearance of P_{on} recapitulate the distribution of lifespans of PP7 activity. In order to calculate PP7 lifespan distribution, PP7 traces are grouped into cohorts according to the maximum measurable

lifespan for each trace (see Methods for details). For each PP7 cohort, a cumulative distribution function (CDF) for the PP7 lifespan is calculated (gray curves). Because the lifespan distribution is truncated at the maximum measurable time, the tails of the CDFs (corresponding to CDF=1) are removed. The solid red line shows the median of these truncated CDFs, which is the cumulative distribution function of lifespans of PP7 activity. The dashed red curve comes from the CDF of an exponential distribution with mean=$(b_2+b_3)^{-1}=(0.014+0.011)^{-1}$min. This exponential CDF is shifted horizontally to account for a deterministic elongation time of 4 min, which coincides with the lifespan of the shortest PP7 trace.

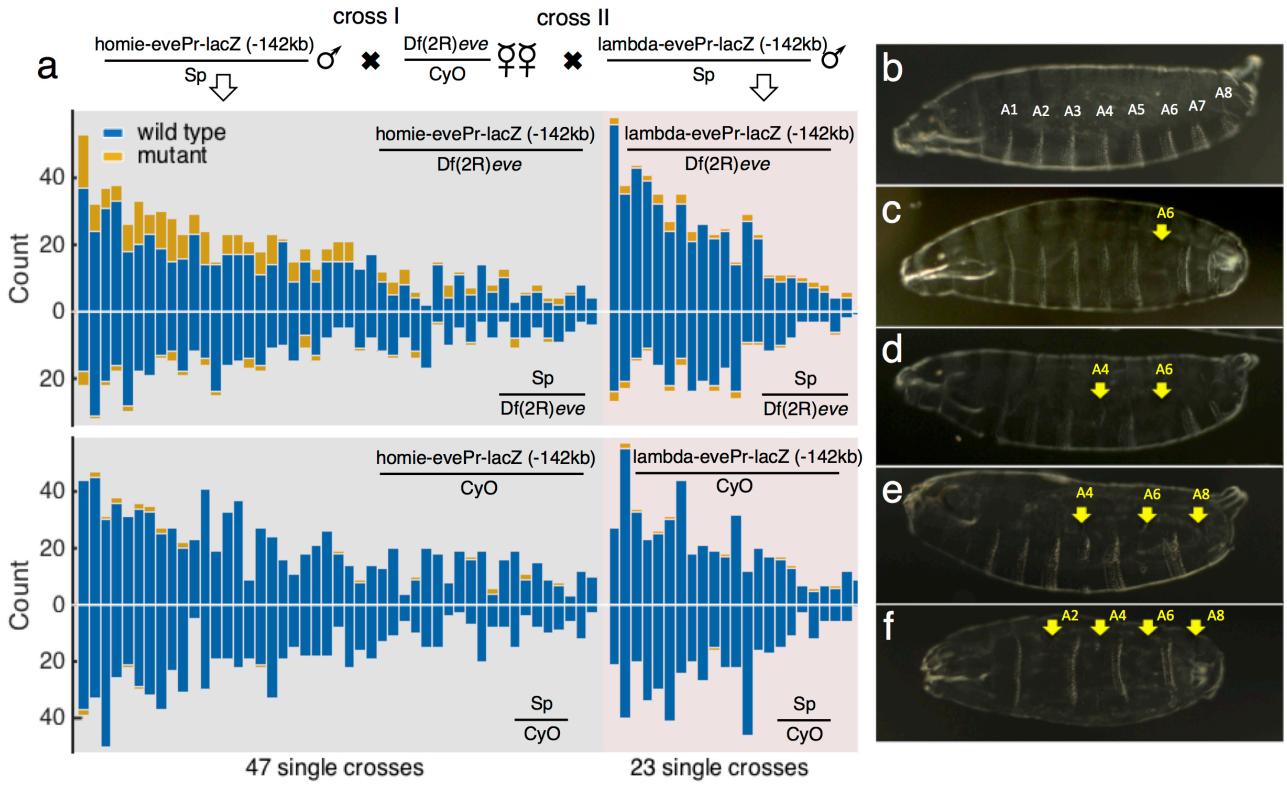

Supplementary Figure 10

Scoring mutant phenotypes resulting from promoter competition.

a, Cross schemes to test phenotypic effects of competition between the endogenous *eve* promoter and the ectopic *eve* promoter that is activated upon the formation of new topological states. Single males, either *homie-evePr-lacZ* or *lambda-evePr-lacZ*, are used for the crosses (note removal of PP7 sequences). For each single cross, the patterning phenotypes in adult abdominal segment A4, A6 and/or A8 are scored. No conspicuous phenotype in other abdominal segments is noticed. **b-f,** The adult abdominal phenotypes most likely result from haploinsufficiency of *eve*, as shown in the cuticles derived from a cross between homozygous *homie-evePr-lacZ* males and *Df*(2R)*eve-/CyO* females. A wild-type cuticle is shown in **b**. Strong *eve* phenotypes, *i.e.* loss or perturbation of denticle bands in the even-numbered abdominal segments, are observed (**c-f**).